A Nature Portfolio journal



https://doi.org/10.1038/s43246-025-00764-9

# Analyzing long-period structural evolution of biaxially stretched ultra-high molecular weight polyethylene films



Hao Zhang ® <sup>1,2,3</sup>, Xincheng Xie<sup>1,3</sup>, Lin Da¹, Yang Liu¹, Caizhen Zhu², Feng Tian ® ¹ ⊠, Xiuhong Li ® ¹ ⊠ & Jian Xu ® ² ⊠

Ultra-high molecular weight polyethylene (UHMWPE) films are widely used in high-performance applications due to their excellent mechanical properties. However, understanding the structural evolution, particularly the long-period structure under tensile fields, remains a challenge in both practical use and processing. Here, we investigate the long-period structural evolution of biaxially stretched UHMWPE films under tensile fields using time-resolved small-angle X-ray scattering. Our results reveal distinct changes in the long-period structure during the stretching process. Initially, the isotropic crystalline regions of UHMWPE align along the stretching direction, transitioning from a diffuse scattering pattern to an ellipsoidal one. As stretching progresses, fibrillar crystals form, dominating the scattering pattern with sharp, oriented features. In the later stages, fragmentation of the fibrillar structure leads to smaller crystalline regions and a butterfly-shaped scattering pattern due to rearranged lamellar structures. Based on these findings, we propose a new model that suggests a reverse transformation from fibrillar crystals to lamellar crystals, contrasting with the traditional "shish-kebab" model. The reduced crystallinity, as shown by differential scanning calorimetry data, further supports this structural transformation.

Since the introduction of the concept of "long-period structure" by Paul J. Flory in his 1969 book "Statistical Mechanics of Chain Molecules", it has served as a crucial bridge for understanding the relationship between the structure and macroscopic properties of polymer materials during processing and application<sup>1</sup>. As for semi-crystalline polymers, it is generally observed that the original spherulitic structure undergoes irreversible deformation from the yield point through to the large strain regime, gradually transforming into a fibrous structure as plastic deformation propagates. This transformation may involve a variety of phenomena, including crystal slip, lamellae fracture, lamellae rotation, and interlamellar shear. Initially, before reaching the yield point, the polymer deforms in an elastic to viscoelastic manner, with structural changes being less pronounced than those observed at large strains2. As deformation continues and the viscoelastic phase concludes, yielding commences, leading to more significant morphological alterations<sup>3</sup>. At this juncture, both the crystalline and amorphous phases exhibit minor orientation changes. With the ongoing increase in strain, the polymer transitions into the large deformation stage, during which the melting and recrystallization of polymer crystals, completed in the previous phase, result in the formation of long-period structures interconnected by flexible amorphous regions. This long-period structure typically induces a hardening phenomenon in the polymer under further strain<sup>4</sup>.

For instance, the "Shish-kebab" structure, characterized by a combination of lamellar and fibrous crystallites, serves as a quintessential model of such long-period structures in typical semicrystalline polymers such as ultra-high-molecular-weight polyethylene (UHMWPE)<sup>5-7</sup>. This structure features a linear core surrounded by plate-like lamellar crystals. Although this "kebab-like" morphology was first observed in the mid-1960s<sup>8</sup>, the mechanisms underlying its formation remain a topic of ongoing debate within the research community. The formation of the lamellar-fibrous structure (Shish-kebab) in UHMWPE is generally attributed to its crystallization in a fluid state<sup>5</sup>; external flow causes orientation and extension of molecules in a polymer melt and thus affects its crystallization kinetics, structure, and morphology<sup>9</sup>. Therefore, this model provides a good description of the long-period structural evolution in materials

processed from the melt through shear, hot pressing, or stretching orientation, such as UHMWPE hot-pressed films, uniaxially stretched UHMWPE films, and UHMWPE fibers 10-13. However, in the case of biaxially stretched UHMWPE films, the material undergoes simultaneous stretching in two directions, resulting in a random arrangement of crystalline regions without significant orientation in any particular direction. This differs from traditional processing methods, such as uniaxial stretching of UHMWPE films or the fabrication of UHMWPE fibers, and leads to variations in the internal structure. Consequently, the applicability of the conventional 'shish-kebab' structural model may be limited in this scenario.

In our previous publication, we employed time-resolved wide-angle X-ray scattering to examine the evolution of the stress-stabilized crystalline structure in biaxially stretched UHMWPE films<sup>14</sup>. In this letter, we extend our investigation to the long-period structure of the same material, The results reveal a unique four-stage evolution pattern of biaxially stretched UHMWPE films (Hereinafter referred to as "BS-UHMWPE" films) under stress, which differs notably from the conventional "shish-kebab" model. This study enhances the understanding of the structure-property relationship between the material's mesoscopic structure and macroscopic performance, supporting the validation of processing methods and performance tuning for specialized applications.

# Result and discussion

In the upper corner of Fig. 1, we show all the TR-SAXS patterns of the dumbbell-shaped (ISO: 37:1994 Type 4) BS-UHMWPE films prepared and stretched at a constant rate of 2 mm/min. Figure 1 presents the complete evolution cycle of BS-UHMWPE membranes at the small-angle scale during tensile deformation until fracture. The long-period structural evolution can be divided into four distinct stages, as illustrated in Fig. 1b. Before stretching, the sample exhibits an isotropic long-period structure scattering signal. As the stretching progresses, the randomly oriented long-period structure gradually transforms into an ordered structure aligned along the stretching direction. With further stretching, sharper fibrillar crystalline scattering patterns appear in the SAXS images. In the later stages of stretching, lamellar signals perpendicular to the stretching direction emerge, forming a "butterfly" SAXS pattern<sup>15</sup>. This long-period evolution pattern differs from that observed in conventionally prepared UHMWPE films via hot pressing (Fig. 1c). In hot-pressed UHMWPE films when stretched to the point of fracture, the SAXS signal reveals only two states: transitioning from a randomly oriented structure to a lamellar-like configuration. Given the extensive studies on the long-period structural evolution of hot-pressed membranes during tensile deformation, further discussion on this aspect will not be provided here<sup>16-18</sup>. Notably, the structural evolution of BS-UHMWPE membranes during tensile deformation is not confined to changes in a single direction. Thus, a bidirectional structural analysis was performed on the in situ SAXS experimental data for these membranes. To enhance clarity, this study introduces the concepts of "polar direction" and "equatorial direction", supplemented by a schematic representation of the corresponding integration regions, as illustrated in Fig. 1d.

First, integration of the 2D SAXS images along the equatorial direction yields one-dimensional SAXS curves for the BS-UHMWPE membranes during the strain process, within a scattering vector range of 0.1 to 1.0 nm<sup>-1</sup>. As the stretching process progresses, the volume of the UHMWPE membranes within the detection area gradually decreases. Consequently, the one-dimensional scattering intensity distribution of these samples was normalized and Lorentz-corrected, with the results presented in Fig. 2a, The figure illustrates the normalized Lorentz-corrected strength versus the material strain rate "ɛ". To facilitate further observation and description, a projection image of Fig. 2a is shown in Fig. 2b. As stretching progresses, the regular lamellar crystalline structure in the equatorial direction becomes increasingly prominent. Importantly, the positions of the scattering peaks do not shift with increasing strain, suggesting that the interspacing of the long-period structure in this direction remains constant. The structural parameters of the long-period arrangement can be estimated using the

following formula<sup>19</sup>:

$$d_{ac} = \frac{2\pi}{q_{\text{max}}} \tag{1}$$

Where,  $d_{ac}$  represents the long-period interspacing in the equatorial direction, and  $q_{\rm max}$  denotes the scattering vector at the maximum intensity of the first-order scattering peak. Calculations yield an estimated long-period interspacing of ~16.11 nm. Since the BS-UHMWPE membranes are semi-crystalline polymers, the crystalline thickness in the equatorial direction can be determined using the one-dimensional correlation function<sup>20</sup> (Supplementary Note 1):

$$\gamma(z) = \frac{\int_0^\infty h^2 J(h) \cos(hz) dh}{\int_0^\infty h^2 J(h) dh}$$
 (2)

Where z denotes the location measured along a trajectory normal to the lamellar surfaces, Here, h represents the scattering vector for Lorentz correction, and J(h) denotes the corresponding scattering intensity. For systems with a structure of stacks of lamellae, the correlation function shows characteristic features that allow the long spacing defined as the average thickness of a lamella together with one interlamellar amorphous layer measured along the lamellar normal to be determined

For systems consisting of stacked lamellae, the correlation function exhibits characteristic features that enable the determination of the long spacing, defined as the average combined thickness of a lamella and its adjacent interlamellar amorphous layer, measured along the normal to the lamellae. As illustrated in Fig. 2c, the first maximum of the y(z) function corresponds to the long-period length of the lamellar structure. At this point, the calculated long-period length is 16.05 nm, which closely aligns with the previous rough estimate of 16.11 nm. From a chemical standpoint, the spacing is a result of the polymer chains packing into extended crystalline structures, with the size of the crystalline domains and the amorphous regions depending on the molecular weight of the polymer and the processing conditions. The observed periodicity of ~16 nm is consistent with typical lamellar thicknesses found in highly crystalline polyethylene<sup>21</sup>. The intersection between the tangent to the initial rising part of the onedimensional correlation function (as indicated by the dashed line in Fig. 2d) and the tangent at the top of the first minimum is indicative of the thickness of the amorphous region, where the crystallinity exceeds 50%. At this stage, the thickness of the amorphous region,  $d_a$ , is determined to be 7.01 nm. In contrast, the thickness of the lamellar crystalline region in the equatorial direction is calculated as  $d_c = d_{ac} - d_a = 9.04$  nm.

The structural evolution in the fibrillar crystalline region (polar direction) can also be further analyzed through fitting. Since this direction exhibits more pronounced orientation in the later stages of the stretching process, the Ruland streak method will be employed for integration fitting (the detailed derivation of the formula can be found in Supplementary Note 2)<sup>22,23</sup>:

$$s^2 B_{\pi/2}^2(s) = \frac{1}{I^2} + s^2 B_{\Phi}$$
 (3)

Where  $B_{\Phi}$  represents the deviation angle between the oriented crystalline structure (fibrillar crystals) and the axial direction, while L denotes the length of the oriented crystalline structure.

Therefore, by slicing and fitting the SAXS scattering images along different scattering vector s values, the relationship between  $B_{\pi/2}^2(s)$  and  $s^2$  can be obtained. Since  $B_{\pi/2}^2(s)$  and  $s^2$  form a linear relationship, a linear fit of the resulting data sets allows for the calculation of the fibrillar crystalline length and misorientation angle in the polar direction. This analysis is primarily focused on the mid-to-late stages of the stretching process of UHMWPE films, as no significant oriented structures were observed during the early stages of stretching. Therefore, it is reasoned that at these early stages, the scattering object shape in the polar direction does not conform to the assumptions of this fitting method. The fibrillar crystalline length,

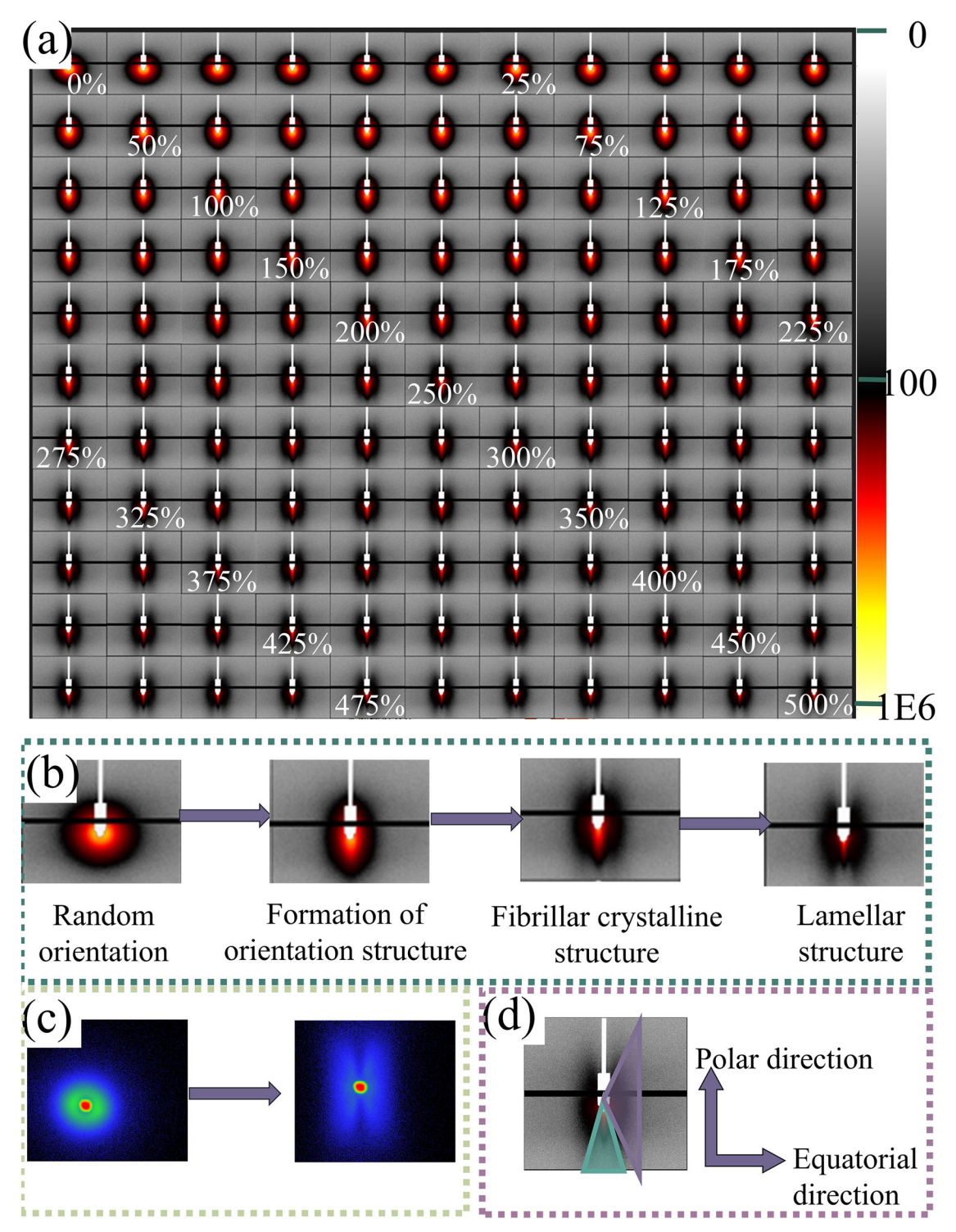


Fig. 1 | In-situ SAXS patterns of BS-UHMWPE under stress fields exhibit a four-stage evolution. a In-situ TR-SAXS pattern (The strain increases from left to right); b SAXS pattern of the long-period structure of BS-UHMWPE film during the stretching process; c SAXS pattern of the long-period structure of thermally pressed

UHMWPE film during the stretching process for comparison;  $\mathbf{d}$  schematic representation of the integrated regions and direction definitions of the scattering pattern of BS-UHMWPE film.

misorientation angle, and the stress–strain curve of the UHMWPE film during stretching, obtained through Ruland streak fitting, are shown in Fig. 2d, e (In figure,  $B_{\Phi}$  represents the deviation angle between the oriented crystalline structure (fibrillar crystals) and the axial direction, while L denotes the length of the oriented crystalline structure).

When analyzing both figures together, it can be observed that during the stress-hardening phase of the stress-strain curve, the fibrillar crystalline length L in the polar direction initially increases and then decreases, reaching a peak at  $\sim\!400\%$  strain. Further stretching leads to the gradual fragmentation of the fibrillar crystals, resulting in the formation of smaller fibrillar crystals. On the other hand, the misorientation angle of the fibrillar crystals, which deviates from the stretching direction, does not follow the same trend as the fibrillar length. Instead, the misorientation angle consistently decreases throughout the stretching process, with its rate of change

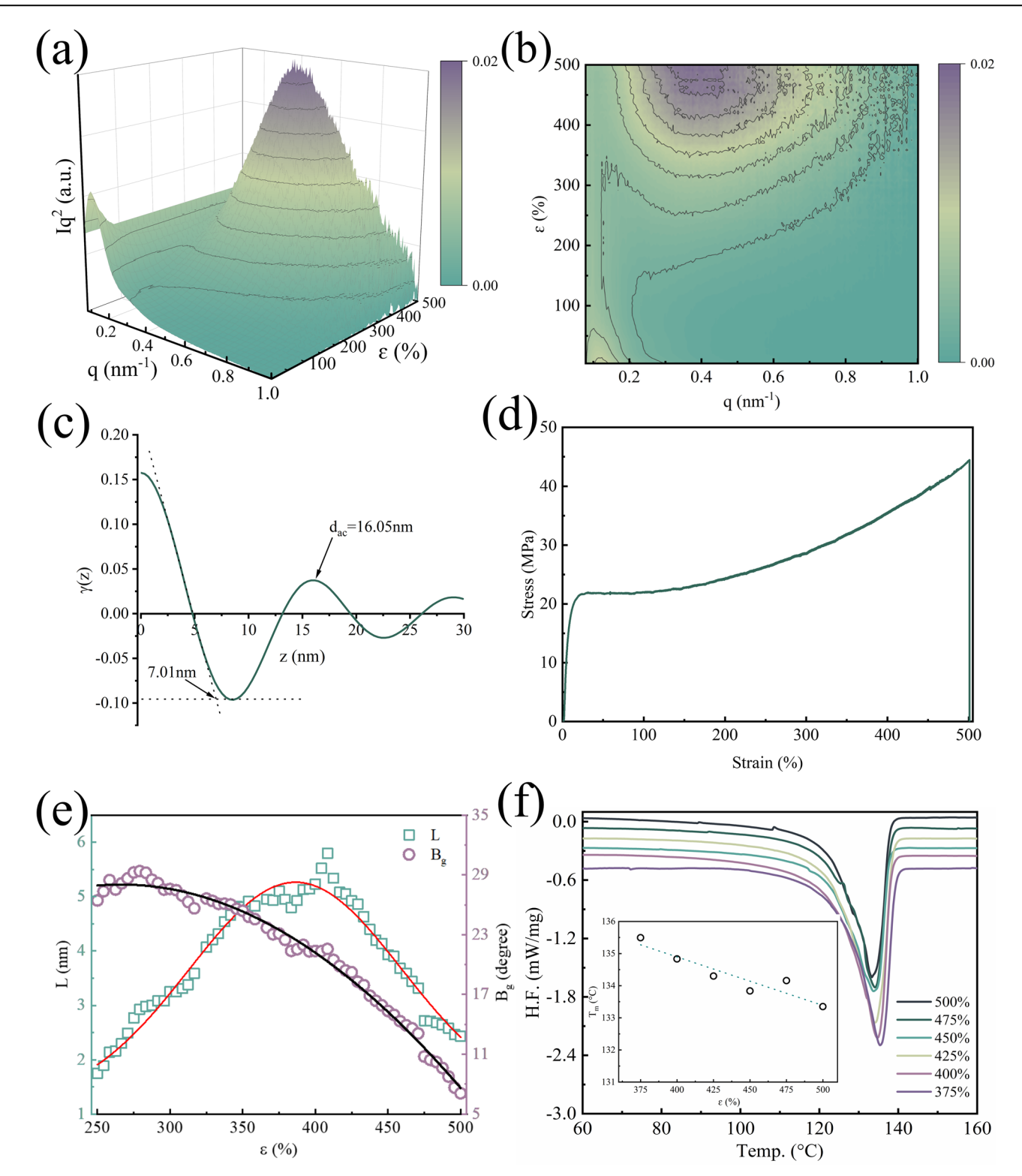


Fig. 2 | The evolution of long-period structure in BS-UHMWPE under stress fields. a Laorenz-corrected one-dimensional SAXS intensity distribution curve; b its projection (b): the vertical projection; c One-dimensional autocorrelation function of UHMWPE film at a strain of 450%; d Stress-strain curve of UHMWPE film during the stretching process (As part of a series of related studies, the mechanical curves from the in-situ synchrotron small-angle scattering tensile

experiments have already been presented in our previous publication<sup>14</sup>); **e** Fiber crystallite length and misorientation angle obtained by Ruland-steak fitting; **f** DSC melting enthalpy curves (Heat flow vs temperature) of UHMWPE material at different stretching ratios, The small figure shows the phase transition temperature points at each strain rate.

accelerating in the later stages of stretching. This phenomenon is partly due to the orientation change induced by tensile strain, and partly because smaller fibrillar crystals, formed after the fragmentation of larger ones, are more easily oriented in the material under continued stretching.

Typically, the formation of the lamellar-fibrillar crystalline structure (Shish-kebab) in UHMWPE materials originates from crystallization in a fluid state<sup>5</sup>. Consequently, many studies have employed this model to analyze and fit UHMWPE films<sup>17</sup>. A distinguishing feature of the Shish-

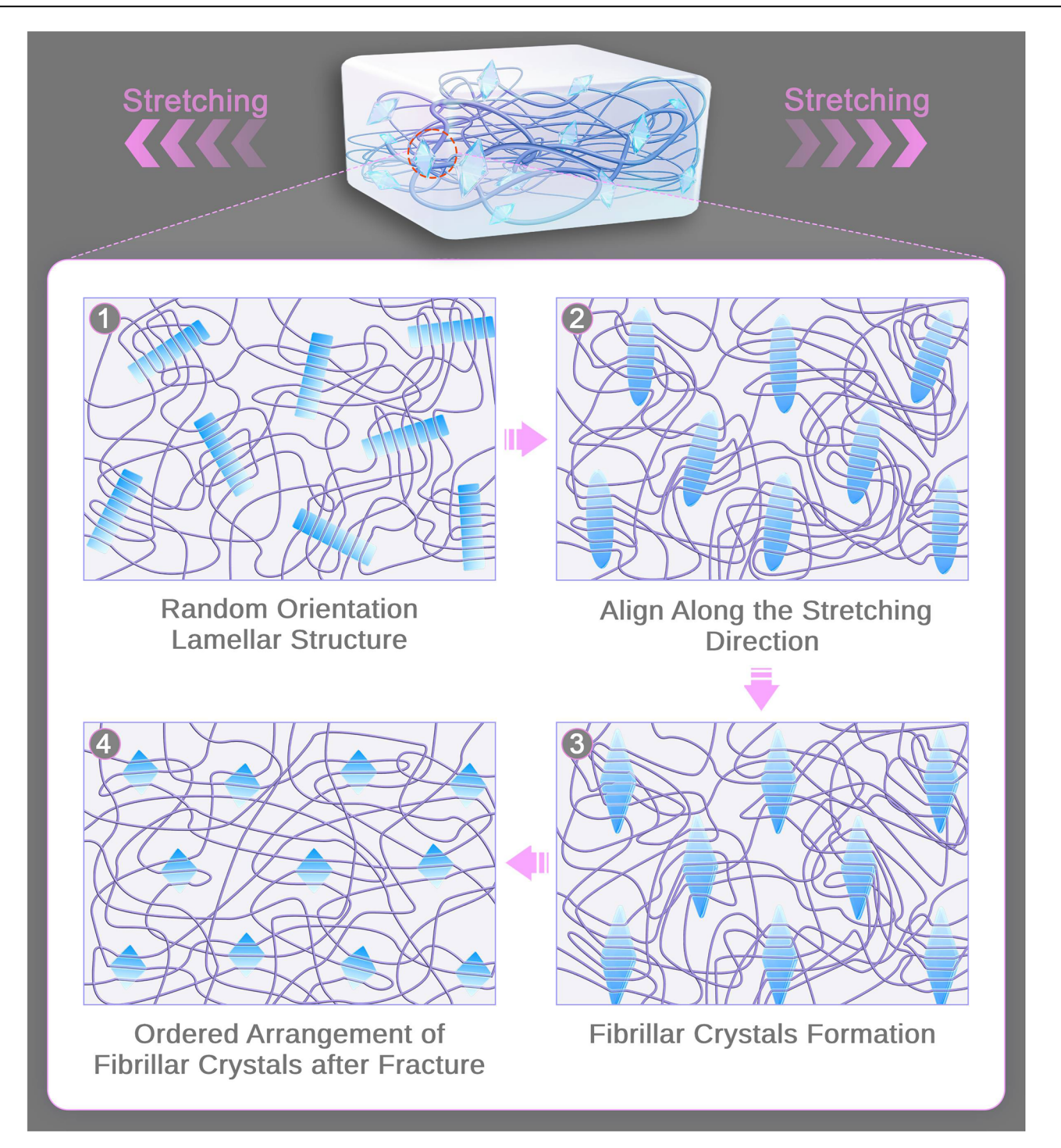


Fig. 3 | Schematic representation of the variation model of the long-period structure of BS-UHMWPE film during the stretching process.

kebab structure is that the length of the "shish" component is significantly greater than that of the "kebab" component<sup>24</sup>. However, the fibrillar crystalline length and lamellar thickness obtained through the aforementioned experiments do not align with the characteristics of the Shish-kebab model. Therefore, this study proposes a new hypothesis: in BS-UHMWPE films, the lamellar and fibrillar crystalline structures originate from the same source and can undergo mutual transformation.

Furthermore, by comparing the evolution data of the lamellar structure in the equatorial direction (as shown in Fig. 2b) with the evolution data of the fibrillar crystalline structure in the polar direction (as shown in Fig. 2e), it can be observed that at around 400% strain, the lamellar content (scattering intensity) gradually increases, while the fibrillar crystals fragment and

decrease in length. This phenomenon may further support the hypothesis proposed in this study, suggesting that during the stretching process of BS-UHMWPE films, a transformation between fibrillar and lamellar structures may occur.

Another potential piece of evidence supporting this hypothesis is that if the lamellar and fibrillar crystalline structures originate from the same source and can undergo a mutual transformation, the overall crystallinity of the material would not significantly increase during the straining process (as no new crystalline structures are being formed). On the other hand, due to the fragmentation of the fibrillar crystalline regions, the conversion rate would not reach 100%, leading to a decrease in the overall crystallinity of the material as strain increases. This hypothesis is confirmed by the DSC

experiment results shown in Fig. 2f. In the DSC experiment, the endothermic heat flow primarily reflects the melting of the crystalline regions in BS-UHMWPE films under different draw ratios. As seen in Fig. 2f, the melting transition point shifts forward as the draw ratio increases, a phenomenon believed to be related to the reduction in the material's crystallinity.

For possible explanations of this phenomenon, some studies have suggested that in highly entangled environments, the severe entanglement of the amorphous regions between lamellae can hinder the formation of new crystals, thereby reducing the probability of crystal nucleation. Under tensile fields, the probability of breaking the highly entangled network is relatively low, allowing for less aggregation in both the original and newly formed crystals, thereby limiting secondary crystal growth<sup>18</sup>.

Based on the above experimental results and hypotheses, this study proposes a model for the long-period evolution of BS-UHMWPE films during the stretching process to explain the long-period structural changes under tensile stress. As shown in Fig. 3, in the initial stretching phase, the BS-UHMWPE film exhibits uniformly arranged crystalline regions, reflected in the SAXS images as a diffuse, circular scattering pattern with no discernible order. As stretching progresses, the uniformly distributed crystalline regions begin to align along the stretching direction, and the SAXS images display an ellipsoidal scattering pattern oriented in the direction of the stretch.

Subsequently, the crystalline regions within the BS-UHMWPE film undergo an orientation transformation, leading to the formation of fibrillar crystals, as indicated by sharp, oriented scattering patterns in the SAXS images, through fitting, we observed that the fibrillar crystal length gradually increased from an initial value of 2 nm to a maximum of ~6 nm. In the midto-late stages of stretching, the fibrillar crystalline structure begins to fracture, with smaller crystalline regions exhibiting a faster rate of dislocation angle change. This suggests a rapid reorientation process in the smaller crystalline regions. The rearranged, regularly oriented lamellar structure formed during this process leads to a "butterfly-shaped" scattering pattern in the SAXS images. In the later stages of stretching, due to the high degree of entanglement in the material, the increased resistance to crystalline motion prevents any significant changes in the overall long-period structure, The long-period dimension was found to be ~16 nm. At the same time, the reduced secondary crystal growth and the fragmentation of the crystalline regions contribute to a decrease in the overall crystallinity of the material.

### Conclusion

In conclusion, based on the TR-SAXS fitting results of BS-UHMWPE film under tensile fields, this study proposes a potential model to describe the evolution of the long-period structure. Unlike the conventional "shish-kebab" model, this model describes the possible reverse transformation from fibrillar crystals to lamellar crystals in BS-UHMWPE films under tensile stress. We hope that this research will contribute to a better understanding of the structural evolution during the processing and application of BS-UHMWPE films, and support the validation of processing methods and performance tuning for specialized applications.

### Methods

The biaxially stretched UHMWPE film was supplied by Goodfellow Group Co. (thickness: 0.075 mm, Mw:  $6\times10^6$  g/mol, UK), The samples were prepared through simultaneous stretching along both the X and Y directions at the same time. (the schematic preparation method shown in Supplementary Fig. 2). Prior to the experiment, which simulates the stress field in a real-world application environment, the samples were immersed in ethanol to remove surface dust and any potential residual solvents. As a comparison, UHMWPE membranes were prepared from UHMWPE resin (Mw:  $5.7\times10^6$  g/mol), supplied by Shanghai Lianle Corporation. The membranes were fabricated using a vacuum hot press (SY6210-ZB, Shiyan Precision Instruments Co., Ltd.) at  $160\,^{\circ}\text{C}$  and  $10\,\text{MPa}$  for 1 h. The tensile experiments were conducted at room temperature using an in-house designed synchrotron radiation in-situ setup, manufactured by INSTEC. The device schematic and setup are shown in Supplementary Fig. 1. This setup was

designed to simulate the material's evolution under realistic stress conditions.

The lattice information of the material has been previously disclosed <sup>14</sup>. In its initial state, the material's wide-angle diffraction shows a relatively orderly orthorhombic crystal form, suggesting that the possibly residual stresses likely have minimal impact on the synchrotron small-angle X-ray scattering results. Time-resolved small-angle X-ray scattering (TR-SAXS) was employed to investigate microstructural changes occurring at larger length scales, enabling an in-depth analysis of the relationship between applied stress and the resulting morphological adaptations in BS-UHMWPE films. The TR-SAXS data were acquired at the 10U1 beamline of the Shanghai Synchrotron Radiation Facility. Comprehensive characterization and fitting analyses were performed on the two-dimensional small-angle scattering patterns using various computational methods, allowing us to elucidate the anisotropic characteristics of the long-period structure. This approach provided detailed insights into the structural evolution along two distinct orientations.

# **Data availability**

All relevant data are available from the authors upon request.

Received: 18 November 2024; Accepted: 24 February 2025; Published online: 04 March 2025

### References

- Flory, P. J. & Volkenstein, M. Statistical mechanics of chain molecules. Biopolymers 8, 699–700 (1969).
- Xiong, B. et al. Amorphous phase modulus and micro-macro scale relationship in polyethylene via in situ SAXS and WAXS. *Macromolecules* 48, 2149–2160 (2015).
- Jiang, Z. et al. Two lamellar to fibrillar transitions in the tensile deformation of high-density polyethylene. *Macromolecules* 43, 4727–4732 (2010).
- Kishimoto, M., Mita, K., Ogawa, H. & Takenaka, M. Effect of submicron structures on the mechanical behavior of polyethylene. *Macromolecules* 53, 9097–9107 (2020).
- Kimata, S. et al. Molecular basis of the Shish-Kebab morphology in polymer crystallization. Science 316, 1014–1017 (2007).
- Tian, Y. et al. Lamellae break-induced formation of shish-kebab during hot stretching of ultra-high molecular weight polyethylene precursor fibers investigated by in situ small angle X-ray scattering. *Polymer* 55, 4299–4306 (2014).
- Tian, Y., Zhu, C., Gong, J., Ma, J. & Xu, J. Transition from shish-kebab to fibrillar crystals during ultra-high hot stretching of ultra-high molecular weight polyethylene fibers: In situ small and wide angle X-ray scattering studies. Eur. Polym. J. 73, 127–136 (2015).
- Binsbergen, F. L. Orientation-induced nucleation in polymer crystallization [16]. Nature 211, 516–517 (1966).
- Somani, R. H., Yang, L., Zhu, L. & Hsiao, B. S. Flow-induced shishkebab precursor structures in entangled polymer melts. *Polymer* 46, 8587–8623 (2005).
- Zhang, Q. et al. Constructing highly oriented and condensed shishkebab crystalline structure of HDPE/UHMWPE blends via intense stretching process: achieving high mechanical properties and inplane thermal conductivity. *Polymer* 241, 124532 (2022).
- Zhang, F., Pan, X., Li, F., Xu, J. & He, X. Shish-kebab structure evolution of HDPE/UHMWPE during hot drawing. *Polym. Eng. Sci.* 64, 2854–2867 (2024).
- Keum, J. K., Zuo, F. & Hsiao, B. S. Formation and stability of shearinduced shish-kebab structure in highly entangled melts of UHMWPE/HDPE blends. *Macromolecules* 41, 4766–4776 (2008).
- Zhou, M., Fan, M., Zhao, Y., Jin, T. & Fu, Q. Effect of stretching on the mechanical properties in melt-spun poly(butylene succinate)/ microfibrillated cellulose (MFC) nanocomposites. *Carbohydr. Polym.* 140, 383–392 (2016).

- Zhang, H. et al. Stress-stabilized crystalline phases of ultrahigh molecular weight polyethylene under tensile stress. ACS Macro Lett. 12, 1379–1383 (2023).
- Wang, W., Murthy, N. S. & Grubb, D. T. "Butterfly" small-angle X-ray scattering patterns in semicrystalline polymers are double-elliptical. *Polymer* 48, 3393–3399 (2007).
- Deng, B., Chen, L., Zhong, Y., Li, X. & Wang, Z. The effect of temperature on the structural evolution of ultra-high molecular weight polyethylene films with pre-reserved shish crystals during the stretching process. *Polymer* 267, 4600–4613 (2023).
- Deng, B., Chen, L., Li, X. & Wang, Z. Influence of prereserved shish crystals on the structural evolution of ultrahigh-molecular weight polyethylene films during the hot stretching process. *Macromolecules* 55, 4600–4613 (2022).
- Chen, L., Deng, B., Li, X. & Wang, Z. Structural evolution of UHMWPE gel fibers as high degree plasticized system during stretching: An in-situ wide and small angle X-ray scattering study. *Polymer* 255, 125149 (2022).
- Qiao, Y. et al. Spontaneous form II to I transition in low molar mass polybutene-1 at crystallization temperature reveals stabilization role of intercrystalline links and entanglements for metastable form II crystals. *Macromolecules* 51, 8298–8305 (2018).
- Qiao, Y. & Men, Y. Intercrystalline links determined kinetics of form II to I polymorphic transition in polybutene-1. *Macromolecules* 50, 5490–5497 (2017).
- Hu, X.-P. & Hsieh, Y.-L. Crystallite sizes and lattice distortions of gelspun ultra-high molecular weight polyethylene fibers. *Polym. J.* 30, 771–774 (1998).
- Thünemann, A. F. & Ruland, W. Microvoids in polyacrylonitrile fibers: a small-angle X-ray scattering study. *Macromolecules* 33, 1848–1852 (2000).
- Zhang, H. et al. Orientation evaluation of ultra-high molecular weight polyethylene fibers: previous studies and an improved method. *J. Appl. Crystallogr.* 55, 876–881 (2022).
- Hsiao, B. S., Yang, L., Somani, R. H., Avila-Orta, C. A. & Zhu, L. Unexpected Shish-Kebab structure in a sheared polyethylene melt. *Phys. Rev. Lett.* 94, 117802 (2005).

### **Acknowledgements**

The authors are grateful for the support from the National Key R&D Program of China (No. 2020YFA0405802).

# **Author contributions**

Hao Zhang: writing-original draft, writing-review & editing. Xincheng Xie: writing-original draft, writing-review & editing. Lin Da: software, validation

Yang Liu: formal analysis Caizhen Zhu: resources, conceptualization Feng Tian: resources, conceptualization, funding acquisition Xiuhong Li: project administration, funding acquisition Jian Xu: funding acquisition, conceptualization.

## **Competing interests**

The authors declare no competing interests.

### **Additional information**

**Supplementary information** The online version contains supplementary material available at https://doi.org/10.1038/s43246-025-00764-9.

**Correspondence** and requests for materials should be addressed to Feng Tian, Xiuhong Li or Jian Xu.

**Peer review information** Communications Materials thanks Wonchalerm Rungswang and the other, anonymous, reviewer(s) for their contribution to the peer review of this work. Primary Handling Editors: Jet-Sing Lee.

**Reprints and permissions information** is available at http://www.nature.com/reprints

**Publisher's note** Springer Nature remains neutral with regard to jurisdictional claims in published maps and institutional affiliations.

Open Access This article is licensed under a Creative Commons Attribution-NonCommercial-NoDerivatives 4.0 International License, which permits any non-commercial use, sharing, distribution and reproduction in any medium or format, as long as you give appropriate credit to the original author(s) and the source, provide a link to the Creative Commons licence, and indicate if you modified the licensed material. You do not have permission under this licence to share adapted material derived from this article or parts of it. The images or other third party material in this article are included in the article's Creative Commons licence, unless indicated otherwise in a credit line to the material. If material is not included in the article's Creative Commons licence and your intended use is not permitted by statutory regulation or exceeds the permitted use, you will need to obtain permission directly from the copyright holder. To view a copy of this licence, visit http://creativecommons.org/licenses/bync-nd/4.0/.

© The Author(s) 2025